Simulation of Drucker–Prager granular flows inside Newtonian fluids

Gilles Daviet, Florence Bertails-Descoubes

▶ **To cite this version:**

Gilles Daviet, Florence Bertails-Descoubes. Simulation of Drucker–Prager granular flows inside Newtonian fluids. 2017. hal-01458951

HAL Id: hal-01458951
https://inria.hal.science/hal-01458951

Preprint submitted on 13 Feb 2017

HAL is a multi-disciplinary open access archive for the deposit and dissemination of scientific research documents, whether they are published or not. The documents may come from teaching and research institutions in France or abroad, or from public or private research centers.

L'archive ouverte pluridisciplinaire **HAL**, est destinée au dépôt et à la diffusion de documents scientifiques de niveau recherche, publiés ou non, émanant des établissements d'enseignement et de recherche français ou étrangers, des laboratoires publics ou privés.

Simulation of Drucker–Prager granular flows inside Newtonian fluids

Gilles Daviet[1] and *Florence* Bertails-Descoubes[1,⋆]

[1] *Inria Rhône-Alpes and Laboratoire Jean Kuntzmann (Grenoble University, CNRS)*

Abstract. Granular-fluid interactions appear in a variety of real-life scenarios ranging from immersed avalanches to ash clouds. We present a continuum-based numerical method for the simulation of such phenomena. Our approach avoids the heavy computational cost inherent to a fluid-solid coupling at the grain scale, while still being able to capture the distinctive regimes governing the collapse of an immersed granular column. To the best of our knowledge, the method presented here is the first to combine fully-coupled two-phase equations for immersed granular flows with an implicit nonsmooth treatment of the Drucker–Prager rheology.

1 Introduction

The dynamical behavior of a granular medium may be largely influenced by its interactions with a surrounding fluid — consider, for instance, the dynamics of an ash cloud in air or of an underwater avalanche. Here, we attempt to predict numerically the qualitative effect that the fluid may exert on the granular material, by modeling the coupled system as two continua. This corresponds to an extension of our recent work on the numerical modeling of dry (single-phase) granular flows [1].

One important feature that want to capture is the ability of a granular avalanche to come eventually at rest, due to static friction between grains. We thus assume the existence of a critical value $\phi^{\max}$ such that when the volume fraction of grains ϕ reaches $\phi^{\max}$, grains interact together through dry frictional contact.

Many authors have proposed to simulate the coupled dynamics of grains in a Newtonian fluid using a two-continua model, but in a restrictive settings and/or using a regularization of the Drucker–Prager yield stress, see, e.g., [2, 3]. Similarly to previous work, our diphasic model relies upon the framework of Jackson [4]. However, unlike previous work, we tackle the yield stress implicitly and without any regularization.

2 Two-continua model

We consider a suspension of particles with diameter D_g in a Newtonian fluid with viscosity η_f. We assume that the fluid occupies the entirety of the volume where there are no grains. That is, the density of the granular phase is $\varrho_g(\phi) = \rho_g\phi$, and the density of the fluid phase is $\varrho_f(\phi) = \rho_f(1-\phi)$. We also suppose that no mass transfer occurs between the two phases (i.e., no chemical reaction).

Notation. Quantities associated with the granular phase will be denoted with a "g" subscript (e.g., $\boldsymbol{u}_g$ will be the velocity field of the grains), while those associated with the surrounding fluid will be denoted with a "f" subscript. The total density of the mixture is thus $\varrho(\phi) = \varrho_f(\phi) + \varrho_g(\phi)$. We also define two velocities for the mixture: the mass-averaged velocity, $\boldsymbol{u}_{\mathrm{m}}$, such that $\varrho(\phi)\boldsymbol{u}_{\mathrm{m}} = \varrho_g(\phi)\boldsymbol{u}_g + \varrho_f(\phi)\boldsymbol{u}_f$, and the volume-averaged velocity, $\boldsymbol{u}_{\mathrm{v}} := \phi\boldsymbol{u}_g + (1-\phi)\boldsymbol{u}_f$.

2.1 Conservation equations

We start from the conservation of mass and momentum for each phase, and express the stresses and momentum transfer terms. Assuming that the sole external force applied to the diphasic medium is gravity, these equations read

$$\rho_g\phi\frac{D_{\boldsymbol{u}_g}\boldsymbol{u}_g}{D_{\boldsymbol{u}_g}t} - \nabla\cdot\left[\boldsymbol{\sigma}_g\right] = \rho_g\phi\boldsymbol{g} + \boldsymbol{f}_{f\to g} \tag{1}$$

$$\rho_f(1-\phi)\frac{D_{\boldsymbol{u}_f}\boldsymbol{u}_f}{D_{\boldsymbol{u}_f}t} - \nabla\cdot\left[\boldsymbol{\sigma}_f\right] = \rho_f(1-\phi)\boldsymbol{g} - \boldsymbol{f}_{f\to g} \tag{2}$$

$$\frac{\partial\phi}{\partial t} + \nabla\cdot\left[\phi\boldsymbol{u}_g\right] = 0 \tag{3}$$

$$\frac{\partial(1-\phi)}{\partial t} + \nabla\cdot\left[(1-\phi)\boldsymbol{u}_f\right] = 0. \tag{4}$$

Expressions for the stresses $\boldsymbol{\sigma}_{f,g}$ and the interfacial momentum transfer $\boldsymbol{f}_{f\to g}$ term remain to be written. To this aim, we use the framework of Jackson [4], and state that the interfacial momentum transfer should consist of a drag term $\boldsymbol{f}^d_{f\to g}$ and a *generalized buoyancy* contribution $\boldsymbol{f}^b_{f\to g}$, such that $\boldsymbol{f}_{f\to g} := \boldsymbol{f}^d_{f\to g} + \boldsymbol{f}^b_{f\to g}$.

Pore stress

Terzaghi's principle [5] states that the total stress of the mixture satisfies $\boldsymbol{\sigma}_f + \boldsymbol{\sigma}_g = \boldsymbol{\sigma}_p + \phi\boldsymbol{\sigma}^C$, where $\phi\boldsymbol{\sigma}^C$ corresponds to the supplemental stress due to the contacts between grains (a.k.a., the *effective* stress), and $\boldsymbol{\sigma}_p$ is the interstitial (or *pore*) stress which can be deduced from the

⋆e-mail: {gilles.daviet,florence.descoubes}@inria.fr

fluid phase stress using $\boldsymbol{\sigma}_f = (1-\phi)\boldsymbol{\sigma}_p$. We thus have

$$\boldsymbol{\sigma}_g = \phi\boldsymbol{\sigma}_p + \phi\boldsymbol{\sigma}^C \qquad \boldsymbol{\sigma}_f = (1-\phi)\boldsymbol{\sigma}_p.$$

Following [3, 4], we decompose the pore stress as a spherical part p (the *pore pressure*) and a viscous stress relative to the volume-averaged velocity $\boldsymbol{u}_\mathrm{v}$, and assume that the viscosity only depends on the local volume fraction, i.e., $\boldsymbol{\sigma}_p = \eta^\mathrm{eff}(\phi)\,\mathrm{D}(\boldsymbol{u}_\mathrm{v}) - p\mathbb{I}$. As argued in [4], the pore stress gives rise to a generalized buoyancy force $\boldsymbol{f}^b_{f\to g} = -\phi\nabla\cdot\left[(1-\phi)\boldsymbol{\sigma}_p\right] + (1-\phi)\nabla\cdot\left[\phi\boldsymbol{\sigma}_p\right] = \boldsymbol{\sigma}_p\nabla\phi$. We obtain

$$\begin{aligned}\nabla\cdot\boldsymbol{\sigma}_g - \boldsymbol{f}^b_{f\to g} &= \phi\nabla\cdot\left[\eta^\mathrm{eff}\,\mathrm{D}(\boldsymbol{u}_\mathrm{v}) - p\mathbb{I}\right] + \nabla\cdot\left[\phi\boldsymbol{\sigma}^C\right]\\ \nabla\cdot\boldsymbol{\sigma}_f + \boldsymbol{f}^b_{f\to g} &= (1-\phi)\nabla\cdot\left[\eta^\mathrm{eff}\,\mathrm{D}(\boldsymbol{u}_\mathrm{v}) - p\mathbb{I}\right].\end{aligned}$$

Contact stress

Just like in [1], we assume the effective stress to be zero where the volume fraction of grains is below a critical value ϕ^max — i.e., in this case grains are separated. Once this critical volume fraction is reached, we assume that the grains are in solid contact, and prevent any further compaction of the particles through the onset of a pressure $p^C := -\frac{1}{d}\operatorname{Tr}\boldsymbol{\sigma}^C$. Moreover, in this dense regime the tangential stress $\operatorname{Dev}\boldsymbol{\sigma}^C$ and the strain rate of the particulate phase $\dot{\boldsymbol{\varepsilon}}_g$ are set to satisfy the non-associated Drucker–Prager flow rule with friction coefficient μ. These conditions are summarized as

$$\begin{cases} 0 \le p^C \perp \phi^\mathrm{max} - \phi \ge 0 & \\ \operatorname{Dev}\boldsymbol{\sigma}^C = \mu p^C \dfrac{\operatorname{Dev}\dot{\boldsymbol{\varepsilon}}_g}{|\operatorname{Dev}\dot{\boldsymbol{\varepsilon}}_g|} & \text{if } \operatorname{Dev}\dot{\boldsymbol{\varepsilon}}_g \neq \mathbf{0} \text{ (yielded)} \\ |\operatorname{Dev}\boldsymbol{\sigma}^C| \le \mu p^C & \text{if } \operatorname{Dev}\dot{\boldsymbol{\varepsilon}}_g = \mathbf{0} \text{ (unyielded).}\end{cases} \tag{5}$$

Note that when the pore pressure increases for a given applied load, the contact pressure p^C, and thus the yield stress, decreases. The normal contact stress rigidifies the material, while the pore pressure plays a lubricating role.

Viscous drag

We assume that the Stokes linear friction law holds at the grain scale, and set the viscous friction force to be proportional to the difference in velocity $\boldsymbol{w}$ between the two phases, $\boldsymbol{f}^d_{f\to g} = -\hat{\xi}(\phi)\boldsymbol{w}$, where the drag coefficient $\hat{\xi}$ is a scalar function of the volume fraction. We can deduce this coefficient from the empirical law for the settling velocity of a suspension of grains given by Richardson and Zaki [6], $\hat{\xi}(\phi) = \frac{\phi(\rho_g-\rho_f)g}{(1-\phi)^\nu}w_\infty$, where w_∞ is the settling velocity of a single particle, $w_\infty = \frac{(\rho_g-\rho_f)gD_g^2}{18\eta_f}$. In the remainder of the paper, we do not assume a precise expression for $\hat{\xi}$, but simply write that $\boldsymbol{f}^d_{f\to g} = -\phi(1-\phi)\xi(\phi)\boldsymbol{w}$, and remember that $\xi(\phi)$ in Pa.s.m^{-2} is similar in order of magnitude to $g\frac{\rho_g-\rho_f}{w_\infty(1-\phi)^{\nu+1}} = \frac{\eta_f}{D_g^2}\frac{18}{(1-\phi)^{\nu+1}}$.

2.2 Dimensionless equations

We first use linear combinations of (1–2) to obtain equations on the mass-averaged velocity $\boldsymbol{u}_\mathrm{m}$ and the fluctuation velocity $\boldsymbol{w}$. To lighten notations, we introduce the scaled density difference $\alpha := \frac{\rho_g-\rho_f}{\rho_f}$. Note that $\rho_g/\rho_f = (\alpha+1)$. Let $\beta(\phi) := (1+\alpha\phi)$, so that the total density of the mixture is given by $\varrho(\phi) = \phi\rho_g + (1-\phi)\rho_f = \beta(\phi)\rho_f$. Let $\pi(\phi) := \phi(1-\phi)$.

The conservation equation for the total momentum of the mixture reads

$$\begin{aligned}\rho_f\left[\beta\frac{D_{\boldsymbol{u}_\mathrm{m}}\boldsymbol{u}_\mathrm{m}}{D_{\boldsymbol{u}_\mathrm{m}}t} + (\alpha+1)\nabla\cdot\left[\frac{\pi}{\beta}\boldsymbol{w}\otimes\boldsymbol{w}\right]\right] + \nabla p\\ - \nabla\cdot\left[\eta^\mathrm{eff}\,\mathrm{D}(\boldsymbol{u}_\mathrm{m} - \alpha\frac{\pi}{\beta}\boldsymbol{w})\right] - \nabla\cdot\left[\phi\boldsymbol{\sigma}^C\right] = \rho_f\beta\boldsymbol{g},\end{aligned} \tag{6}$$

while the fluctuation momentum conservation reads

$$\begin{aligned}(\alpha+1)\rho_f\phi\left[\frac{\partial\boldsymbol{w}}{\partial t} + \left(\left\{\!\!\left\{\boldsymbol{u}_{f,g}\right\}\!\!\right\}\cdot\nabla\right)\boldsymbol{w} + (\boldsymbol{w}\cdot\nabla)\left\{\!\!\left\{\boldsymbol{u}_{f,g}\right\}\!\!\right\}\right] + \beta\phi\xi\boldsymbol{w}\\ - \alpha\phi\nabla p + \alpha\phi\nabla\cdot\left[\eta^\mathrm{eff}\,\mathrm{D}(\boldsymbol{u}_\mathrm{m} - \alpha\frac{\pi}{\beta}\boldsymbol{w})\right] - \nabla\cdot\left[\phi\boldsymbol{\sigma}^C\right] = \mathbf{0}\end{aligned} \tag{7}$$

where $\left\{\!\!\left\{\boldsymbol{u}_{f,g}\right\}\!\!\right\} := \frac{1}{2}\left(\boldsymbol{u}_g + \boldsymbol{u}_f\right)$. Linear combinations of the mass conservation equations (3–4) also yield

$$\frac{\partial\beta}{\partial t} + \nabla\cdot\left[\beta\boldsymbol{u}_\mathrm{m}\right] = 0 \qquad \nabla\cdot\left[\boldsymbol{u}_\mathrm{m} - \frac{\alpha\pi}{\beta}\boldsymbol{w}\right] = 0. \tag{8}$$

Dimensionless numbers

As we mostly study gravity-driven flows, we define the characteristic mixture velocity as $U := \sqrt{gL}$, where L is a characteristic length of the studied phenomenon. For the same reason, we choose $P := \rho_f gL$ as the characteristic pore pressure, $(\alpha+1)P = \rho_g gL$ as the characteristic contact stress, and $T = \frac{L}{U}$ as the characteristic time. Finally, at the risk of overestimating W, we define the characteristic relative velocity as the settling velocity of a single grain, w_∞. We also introduce dimensionless versions of the effective viscosity and drag fields,

$$\eta^\mathrm{eff} = \eta_f\tilde{\eta^\mathrm{eff}} \qquad \xi = g\frac{\rho_g-\rho_f}{w_\infty}\Xi\tilde{\xi},$$

where the dimensionless number Ξ denotes the order of magnitude of the geometry dependent term in ξ, i.e., $\Xi \sim \xi\frac{w_\infty}{\rho_g-\rho_f}g \sim (1-\phi)^{-\nu-1}$. Note that as ν is usually taken to be greater than 3, Ξ is highly dependent on the target volume fraction.

We introduce two dimensionless number; the Reynolds number of the fluid, Re, and a Stokes number, St, relating the importance of the mixture kinetic energy to the dissipation by drag forces:

$$\mathrm{Re} := \frac{\rho_f UL}{\eta_f} \qquad \mathrm{St} := \frac{W}{U} = \frac{(\rho_g-\rho_f)gD_g^2}{18U\eta_f} = \frac{\rho_g UD_g^2}{18L\eta_f}.$$

The relationship between these dimensionless numbers is given by ratios of density and length, $\mathrm{St} = \frac{\alpha+1}{18}\frac{\rho_f UD_g^2}{L\eta_f} = \frac{\alpha+1}{18}\mathrm{Re}\left(\frac{D_g}{L}\right)^2 = \frac{\alpha+1}{18}\epsilon^2\mathrm{Re}$, where $\epsilon := \frac{D_g}{L}$ denotes the ratio

of the grains diameter to the characteristic length. Equations (6–7) become

$$\frac{\beta}{\alpha+1}\frac{D_{\tilde{\boldsymbol{u}_\mathrm{m}}}\tilde{\boldsymbol{u}_\mathrm{m}}}{D_{\tilde{\boldsymbol{u}_\mathrm{m}}}\tilde{t}} + \mathrm{St}^2\tilde{\nabla}\cdot\left[\frac{\pi}{\beta}\tilde{\boldsymbol{w}}\otimes\tilde{\boldsymbol{w}}\right] - \tilde{\nabla}\cdot\left[\phi\tilde{\boldsymbol{\sigma}}^C\right] - \frac{1}{\alpha+1}\tilde{\nabla}\cdot\left[\frac{\tilde{\eta^{\mathrm{eff}}}}{\mathrm{Re}}\tilde{\mathrm{D}}(\tilde{\boldsymbol{u}_\mathrm{m}} - \mathrm{St}\alpha\frac{\pi}{\beta}\tilde{\boldsymbol{w}}) - \tilde{p}\mathbb{I}\right] = \frac{\beta}{\alpha+1}\boldsymbol{e}_g \quad (9)$$

$$\phi\mathrm{St}\left[\frac{\partial\tilde{\boldsymbol{w}}}{\partial\tilde{t}} + J(\tilde{\boldsymbol{u}_\mathrm{m}},\tilde{\boldsymbol{w}}) + \mathrm{St}J(\frac{1-2\phi-\alpha\phi}{2\beta}\tilde{\boldsymbol{w}},\tilde{\boldsymbol{w}})\right] + \frac{\alpha\beta}{\alpha+1}\phi\Xi\tilde{\xi}\tilde{\boldsymbol{w}} = \frac{\alpha\phi}{\alpha+1}\left(\tilde{\nabla}\tilde{p} - \frac{1}{\mathrm{Re}}\tilde{\nabla}\cdot\left[\tilde{\eta^{\mathrm{eff}}}\tilde{\mathrm{D}}(\tilde{\boldsymbol{u}_\mathrm{m}} - \alpha\mathrm{St}\frac{\pi}{\beta}\tilde{\boldsymbol{w}})\right)\right) + \tilde{\nabla}\cdot\left[\phi\tilde{\boldsymbol{\sigma}}^C\right], \quad (10)$$

where $J(\boldsymbol{v},\boldsymbol{w}) := (\boldsymbol{v}\cdot\tilde{\nabla})\boldsymbol{w} + (\boldsymbol{w}\cdot\tilde{\nabla})\boldsymbol{v}$.

2.3 Discrete-time equations

We consider a discrete timestep $[t^k, t^{k+1} = t + \Delta_t]$. We assume that the total derivative of each phase can be approximated as

$$\frac{D_{\boldsymbol{u}_{f,g}}\boldsymbol{u}_{f,g}}{D_{\boldsymbol{u}_{f,g}}t} = \frac{\boldsymbol{u}_{f,g}(t^{k+1}) - U_{f,g}\circ\boldsymbol{u}_{f,g}(t^k)}{\Delta_t} + O(\Delta_t),$$

where $U_{f,g}$ is a function depending only on the velocity field at the previous timestep (this is the case for instance when using a characteristics or particle-based transport scheme). Moreover, as in [1] we discretize the maximal volume fraction condition $\phi(t^{k+1}) \le \phi^{\max}$ over the timestep using a Lagrangian point-of-view as

$$\phi(t^k) + \phi(t^k)\nabla\cdot\left[\boldsymbol{u}(t^{k+1})\right] \le \phi^{\max},$$

i.e., $\mathrm{Tr}\,\boldsymbol{\gamma} \le 0$ with $\boldsymbol{\gamma} := \phi\dot{\boldsymbol{\varepsilon}} + \frac{\phi^{\max}-\phi(t^k)}{d\,\Delta_t}\mathbb{I}$. The discrete-time version of Eq (5) can thus be expressed as function of only $\boldsymbol{\gamma}$ and $\boldsymbol{\sigma}^C$; using the notation of [1], we write (5) $\iff$ $(\boldsymbol{\gamma}, -\boldsymbol{\sigma}^C) \in \mathcal{DP}_\mu$. We note that in 2D, $\mathcal{DP}_\mu$ is structurally similar to the set of 3D velocity-force solutions to the Coulomb friction law.

We use a semi-implicit integration scheme defined as follows: first, compute the end-of-step velocities and stresses from the conservation of momentum equations subject to the constraints $(\boldsymbol{\gamma}, -\boldsymbol{\sigma}^C) \in \mathcal{DP}_\mu$ and $\nabla\cdot\boldsymbol{u}_\mathrm{v} = 0$; then, update the volume fraction field following the transport equation $\frac{\partial\phi}{\partial t} = -\nabla\cdot\left[\phi\boldsymbol{u}(t^{k+1})\right]$.

Variational formulation

Let us consider a simulation domain Ω, with, for the sake of simplicity, homogeneous Dirichlet boundary conditions. Let as usual V denote a subspace of $H^1(\Omega)^d$ satisfying the boundary conditions, and $T(\Omega) \sim L_2(\Omega)^{\frac{d}{2}(d+1)}$ be the space of square-integrable symmetric tensor fields on Ω. In order to obtain a symmetric system, we perform two last changes of variable. We introduce the scaled fluctuation velocity $\hat{\boldsymbol{w}} := \sqrt{\mathrm{St}}\frac{1-\phi}{\beta}\boldsymbol{w}$, and the symmetric tensor field $\boldsymbol{\lambda} := -\boldsymbol{\sigma}^C$. The first step of our semi-implicit integration scheme consists in finding a solution to the following variational formulation,

Find $\boldsymbol{u}_\mathrm{m}, \hat{\boldsymbol{w}} \in V^2$, $p \in L_2(\Omega)$ and $\boldsymbol{\gamma}, \boldsymbol{\lambda} \in T^2$ such that

$$\begin{array}{rrl} a(\boldsymbol{u}_\mathrm{m},\boldsymbol{v}) + e(\hat{\boldsymbol{w}},\boldsymbol{v}) - b(p,\boldsymbol{v}) & -g(\boldsymbol{\lambda},\boldsymbol{v}) = & l(\boldsymbol{v})\ \forall\boldsymbol{v}\in V \\ e(\boldsymbol{u}_\mathrm{m},\boldsymbol{z}) + r(\hat{\boldsymbol{w}},\boldsymbol{z}) - c(p,\boldsymbol{z}) & -h(\boldsymbol{\lambda},\boldsymbol{z}) = & f(\boldsymbol{z})\ \forall\boldsymbol{z}\in V \\ -b(q,\boldsymbol{u}_\mathrm{m}) - c(q,\hat{\boldsymbol{w}}) & = & 0\ \forall q\in L_2(\Omega) \\ -g(\boldsymbol{\tau},\boldsymbol{u}_\mathrm{m}) - h(\boldsymbol{\tau},\hat{\boldsymbol{w}}) & +m(\boldsymbol{\gamma},\boldsymbol{\tau}) = & k(\boldsymbol{\tau})\ \forall\boldsymbol{\tau}\in T \\ & (\boldsymbol{\gamma},\boldsymbol{\lambda}) \in & \mathcal{DP}_\mu. \end{array} \quad (11)$$

$$a(\boldsymbol{u},\boldsymbol{v}) := \frac{1}{\Delta_t}\int_\Omega\frac{\beta}{\alpha+1}\langle\boldsymbol{u},\boldsymbol{v}\rangle + \int_\Omega\frac{\eta^{\mathrm{eff}}\,\mathrm{D}(\boldsymbol{u}):\mathrm{D}(\boldsymbol{v})}{(\alpha+1)\mathrm{Re}}$$

$$r(\boldsymbol{w},\boldsymbol{z}) := \int_\Omega\frac{\phi\beta}{1-\phi}\left(\frac{\mathrm{St}}{\Delta_t} + \frac{\alpha\beta}{\alpha+1}\Xi\xi\right) + \frac{\mathrm{St}}{\mathrm{Re}}\frac{\alpha^2}{\alpha+1}\int_\Omega\eta^{\mathrm{eff}}\,\mathrm{D}(\phi\boldsymbol{w}):\mathrm{D}(\phi\boldsymbol{z})$$

$$e(\boldsymbol{w},\boldsymbol{z}) := -\frac{\alpha\sqrt{\mathrm{St}}}{\alpha+1}\int_\Omega\frac{\eta^{\mathrm{eff}}}{\mathrm{Re}}\mathrm{D}(\phi\boldsymbol{w}):\mathrm{D}(\boldsymbol{v}) \quad m(\boldsymbol{\gamma},\boldsymbol{\tau}) := \int_\Omega\boldsymbol{\gamma}:\boldsymbol{\tau}$$

$$b(p,\boldsymbol{v}) := \frac{1}{\alpha+1}\int_\Omega p\nabla\cdot\boldsymbol{z} \quad c(p,\boldsymbol{z}) := \frac{\alpha\sqrt{\mathrm{St}}}{\alpha+1}\int_\Omega\phi\langle\nabla p,\boldsymbol{z}\rangle$$

$$g(\boldsymbol{\tau},\boldsymbol{u}) := \int_\Omega\phi\boldsymbol{\tau}:\mathrm{D}(\boldsymbol{u}) \qquad h(\boldsymbol{\tau},\boldsymbol{u}) := \sqrt{\mathrm{St}}\int_\Omega\phi\boldsymbol{\tau}:\mathrm{D}(\boldsymbol{w})$$

$$l(\boldsymbol{v}) := \int_\Omega\frac{\beta\left\langle\boldsymbol{e}_g,\boldsymbol{v}\right\rangle}{\alpha+1} + \left\langle(\alpha+1)\phi U_g(\boldsymbol{u}_g^k) + (1-\phi)U_f(\boldsymbol{u}_f^k), \frac{\boldsymbol{v}}{\Delta_t}\right\rangle$$

$$k(\boldsymbol{\tau}) := \int_\Omega\frac{\phi^{\max}-\phi}{\Delta_t}\frac{\mathrm{Tr}\,\boldsymbol{\tau}}{d}$$

$$f(\boldsymbol{z}) := \frac{\sqrt{\mathrm{St}}}{\Delta_t}\int_\Omega\phi\left\langle U_g(\boldsymbol{u}_g^k) - U_f(\boldsymbol{u}_f^k), \boldsymbol{z}\right\rangle.$$

where $\langle\cdot,\cdot\rangle$ denotes the usual scalar product on $\mathbb{R}^d$.

2.4 Discrete equations

Choosing adequate discrete spaces for our variables, and expressing the constraints on quadrature points (see [1]), the vectors of coefficients for our fields (underlined) have to satisfy

$$\begin{cases} A\underline{\boldsymbol{u}} + E^\intercal\underline{\boldsymbol{w}} = \underline{\boldsymbol{l}} + B^\intercal\underline{\boldsymbol{p}} + G^\intercal\underline{\boldsymbol{\lambda}} \\ E\underline{\boldsymbol{u}} + R\underline{\boldsymbol{w}} = \underline{\boldsymbol{f}} + C^\intercal\underline{\boldsymbol{p}} + H^\intercal\underline{\boldsymbol{\lambda}} \\ \mathbf{0} = B\underline{\boldsymbol{u}} + C\underline{\boldsymbol{w}} \\ \underline{\boldsymbol{\gamma}} = \underline{\boldsymbol{k}} + G\underline{\boldsymbol{u}} + H\underline{\boldsymbol{w}} \\ (\underline{\boldsymbol{\lambda}}_{[i]}, \underline{\boldsymbol{\gamma}}_{[i]}) \in \mathcal{DP}_\mu \quad \forall i. \end{cases} \quad (12)$$

This system is structurally similar to the ones arising from Discrete Element Modeling with Coulomb friction and linear kinematic constraints. We can thus leverage the efficient solvers that have been devised for this purpose.

While many discretization strategies may be envisoned, in practice we follow our previous approach [1]. That is, we discretize Eq (11) in space using the Material Point Method, then solve Eq (12) using our two-step process and a Gauss–Seidel solver.

3 Results

We have reproduced the immersed column collapses presented in [7], in which a DEM method is coupled with a fluid simulation. In our continuum-based approach, we use the $\mu(I)$ rheology to model frictional contacts, with $\mu_S = 0.32$ and $\mu_D = 0.6$.

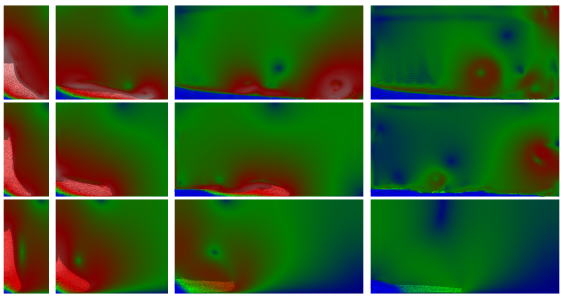

Figure 1. Snapshots at identical instants of the collapse of a granular column in three different fluids: air (top), water (middle), and viscous (bottom). Colors indicate the particle and fluid velocities, on the same scale (blue is slowest, white fastest).

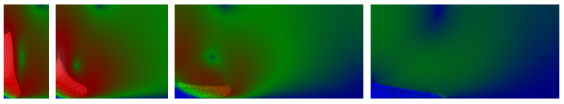

Figure 2. Granular column collapse in the viscous (bottom) fluid of Figure 1 with triple-sized grains.

We consider a 2D granular column of aspect-ratio $a = 8$, with grains of diameter $D_g = 1$mm and volumetric mass $\rho_g = 2600\text{kg.m}^{-3}$. The column width is $W = 11.5D_g$. As in [7], we consider three choices for the surrounding fluid: (1.) *air*: $\rho_f = 1\text{kg.m}^{-3}$ and $\eta_f = 10^{-5}$Pa.s; (2.) *water*: $\rho_f = 1000\text{kg.m}^{-3}$ and $\eta_f = 10^{-3}$Pa.s; and (3.) *viscous*: $\rho_f = 1000\text{kg.m}^{-3}$ and $\eta_f = 1$Pa.s. Numerical simulations in [7] yield a different collapse regime for each of these choices, which Topin et al. respectively coin *grain-inertial*, *fluid-inertial*, and *viscous*. In the latter case, the collapse is simply slowed-down by the fluid, and the run-out length is much shorter than in the dry (i.e., grain-inertial) case. In the fluid-inertial regime, the kinetic energy initially transferred from the grains to the fluid is transferred back to the grains in the later stage of the collapse, maintaining an horizontal velocity for a much longer time than in the two other regimes. As such, the final run-out length in the fluid-inertial regime can surpass that of the dry case. As shown in Figure 1, in the (1.) and (2.) cases we retrieve the grain-inertial and fluid-inertial regimes. Case (3.) remains however mostly in the fluid-inertial regime; albeit much slower than the collapse in water, the collapse in the viscous fluid achieves a barely shorter run-out length. While initially surprising, this can be explained by looking at the characteristic numbers of our model. To determine which regime drives the flow, we can look at the ratio between two timescales: the one for the viscous collapse, $T_v := \eta_f/\rho_f g L$, where L is the height of the basin, and the other for the grains to come into contact, $T_c := D_g/W$,

$$\frac{T_v}{T_c} = \frac{\eta_f W}{\rho_f g L D_g} = \frac{\eta_f \text{St} U}{\rho_f U^2 L \epsilon} = \frac{\text{St}}{\text{Re}\epsilon} = \frac{\alpha+1}{18}\epsilon.$$

Rather than the Reynolds number, the value of $(\alpha+1)\epsilon$ is the one that determines the regime of the collapse; the fluid-inertial collapse will occur when T_v/T_c is sufficiently small. For our column, $\epsilon = 10^{-2}$; in the dry case, $\alpha = 2599$ and thus $T_v/T_c \sim 1$; the collapse is therefore quickly stabilized by the contact forces. However, this number remains constant for the choice of parameters (2.) and (3.), $\alpha\epsilon \sim 10^{-3}$. One solution to model a viscous collapse is thus to increase ϵ, i.e., to consider larger grains. With our simulator, starting from the choice of parameters (3.) and simply tripling the diameters of the particles allows us to reduce the duration and run-out length of the collapse significantly (see Figure 2).

Discussion

Our approach currently suffers from a number of limitations. First, our model of the drag term in the interfacial momentum transfer term is not sufficient to retrieve the transition between the fluid-inertial and viscous regimes predicted by discrete simulations. A nonlinear dependency of the drag force on the fluid viscosity for higher concentrations of particles may be necessary. Then, another missing ingredient is a dependency on the initial volume fraction of grains, which has been observed to determine the onset of the flow. However, with our drag force a higher volume fraction will mean that the fluid will oppose more resistance to the initial motion of the grains, and thus will make stronger compact granular heaps.

On the positive side, our approach is able to recover the qualitative dynamics of immersed granular flows in different regimes. We are able to capture the duality of the fluid role, which may either lubricate the flow or dampen it, following the relative importance of the pore pressure and contact forces. Moreover, our resulting one-step numerical problem turns out to be standard in discrete contact dynamics with linear constraints, allowing us to leverage the large body of research devoted to such systems.

References

[1] G. Daviet, F. Bertails-Descoubes, ACM Transactions on Graphics **35**, 13 (2016)

[2] J. Chauchat, M. Médale, Computer Methods in Applied Mechanics and Engineering **199**, 439 (2010)

[3] J. Chauchat, S. Guillou, D. Pham Van Bang, K. Dan Nguyen, Journal of Hydraulic Research **51**, 293 (2013)

[4] R. Jackson, *The dynamics of fluidized particles* (Cambridge University Press, 2000)

[5] K. Terzaghi, Proc. 1st International Conference on Soil Mechanics and Foundation Engineering (1936)

[6] J.F. Richardson, W.N. Zaki, Transactions of Institution of Chemical Engineers **32**, 35 (1954)

[7] V. Topin, Y. Monerie, F. Perales, F. Radjaï, Physical Review Letters **109** (2012)